Acta Technica *62*, No. 3B/2017, 277–292

Theoretical and experimental investigation of a passive nonlinear vibration isolator using negative stiffness structure[1]

Ren Xudong[1,2], Meng Lingshuai[1,3], Ren Xudong[1,4]

Abstract. This paper presents a passive nonlinear vibration isolator which is developed by adding the symmetric negative stiffness structure to a vertical air spring. The restoring force and stiffness of the air spring and the proposed nonlinear vibration isolator are derived. The dynamic equations of the proposed nonlinear system and the single air spring system without the negative stiffness structure under harmonic excitation are established. Based on the Harmonic Balance Method, the absolute displacement transmissibility of the two systems is obtained. Considering different excitation amplitudes and damping ratios, effects of the system imperfections on the vibration isolation performance are studied.

Key words. Air spring, negative stiffness, nonlinear vibration isolator.

1. Introduction

Owing to the better vibration isolation performance than linear isolators in low frequency region, passive nonlinear vibration isolators have drawn much attention in the scientific and industrial fields. Ibrahim introduced the recent advances in passive nonlinear vibration isolators and described their main nonlinear characteristics in detail [1]. A comprehensive review on passive nonlinear vibration isolators was presented by Alabuzhev et al. [2], in which a large number of prototypes utilizing negative stiffness structure have resulted in low frequency isolation and excellent support capacity. Carrella et al. proposed a high-static-low-dynamic-stiffness iso-

[1]Institute of Medical Equipment, Academy of Military Medical Sciences, 106 Wandong Road, Hedong District, Tianjin, 300161, China
[2]E-mail: r_xudong@163.com
[3]E-mail: mengls1989@sina.com
[4]E-mail: sunjg@vip.sina.com

lator by connecting a vertical coil spring and two oblique coil springs [3]. Le and Ahn proposed a nonlinear isolator using a horizontal spring in series with a bar as negative stiffness structure [4]. Liu et al. carried out a research on Euler buckled beam to work as negative stiffness corrector to realize a quasi-zero stiffness isolator [5]. Meng et al. proposed a quasi-zero stiffness isolator by combining a disk spring with a vertical linear spring [6].

In this paper, a novel passive nonlinear isolator including a vertical air spring and two symmetric negative stiffness structures is studied. Each negative stiffness structure configured by a horizontal air spring in series with a bar is connected to the vertical air spring in parallel. The reason for using the horizontal air spring to construct the negative stiffness structure is that it can enable the nonlinear forces in horizontal direction to be adjusted flexibly by changing the internal pressure of the air spring. Meanwhile, the negative stiffness structure with the air spring can exhibit strongly nonlinearity. In addition, the vertical air spring can satisfy the practical conditions of variable isolation masses by changing its internal pressure.

2. The characteristics of the air spring

A schematic model of an air spring is shown in Figure 1. The bottom plate of the air spring is fixed, while the upper plate is mobile along the vertical axis under the applied force P. By referring to the article [7], the internal pressure and volume of the air spring satisfy the equation

$$(p + p_{\mathrm{a}})\, V^{\chi} = (p_0 + p_{\mathrm{a}})\, V_0^{\chi}\,, \tag{1}$$

where V is the instantaneous effective volume, V_0 is the initial volume of the air spring in natural state, p is the instantaneous air pressure, p_{a} is the standard atmospheric pressure, p_0 is the air pressure of initial state and χ is the specific heat ratio. The value of χ depends on the deformation velocity of the air spring.

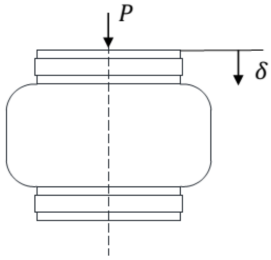

Fig. 1. Schematic representation of the air spring

Then, the restoring force of the air spring can be derived as

$$F = pA_{\mathrm{e}} = \left[\left(\frac{V_0}{V}\right)^{\chi}(p_0 + p_{\mathrm{a}}) - p_{\mathrm{a}}\right] A_{\mathrm{e}}\,, \tag{2}$$

where A_{e} is the effective area of the air spring.

The relationship between the effective area A_e and the instantaneous deflection δ of the air spring can be defined as

$$A_\mathrm{e} = A_0 + \varepsilon\delta\,, \tag{3}$$

where A_0 is the initial area of the air spring at natural state and ε is the rate of change of the effective area with respect to δ.

By differentiating (2) with respect to the instantaneous deflection δ, the stiffness of the air spring can be derived as

$$k = \frac{\mathrm{d}F}{\mathrm{d}\delta} = A_\mathrm{e}\frac{\mathrm{d}p}{\mathrm{d}\delta} + p\frac{\mathrm{d}A_\mathrm{e}}{\mathrm{d}\delta} =$$

$$= -\chi A_\mathrm{e}\left(p_0 + p_\mathrm{a}\right)\frac{V_0^\chi}{V^{\chi+1}}\frac{\mathrm{d}V}{\mathrm{d}\delta} + \left[\left(\frac{V_0}{V}\right)^\chi\left(p_0 + p_\mathrm{a}\right) - p_\mathrm{a}\right]\frac{\mathrm{d}A_\mathrm{e}}{\mathrm{d}\delta}\,. \tag{4}$$

Since the vibration amplitude of the air spring is very small, the following equations can be obtained,

$$\frac{V_0}{V} \approx 1 \;\Rightarrow\; A_\mathrm{e} = -\frac{\mathrm{d}V}{\mathrm{d}\delta}\,. \tag{5}$$

Combining (2)–(5), the stiffness of the air spring k can be derived as

$$k = \frac{\chi\varepsilon^2\left(p_0 + p_\mathrm{a}\right)}{V}\delta^2 + \frac{2\chi\varepsilon A_0\left(p_0 + p_\mathrm{a}\right)}{V}\delta + \frac{\chi A_0^2\left(p_0 + p_\mathrm{a}\right)}{V} + p\varepsilon\,. \tag{6}$$

It can be seen obviously that the stiffness of the air spring is the quadratic polynomial of the deflection. Then, the restoring force of the air spring can be derived to be the cubic polynomial of the deflection as follow

$$F = k_3\delta^3 + k_2\delta^2 + k_1\delta + F_0\,, \tag{7}$$

where k_1, k_2 and k_3 are the stiffness coefficients, and F_0 is constant.

Then, the stiffness of the air spring can be expressed by

$$k = 3k_3\delta^2 + 2k_2\delta + k_1\,. \tag{8}$$

2.1. Experiment of the air spring

To measure the restoring force pertaining to the deflection, an experiment was carried out by applying the axial force on the air spring. The air spring used in the experiment is the 086060H-1 type manufactured by Xi'an Chenguang Rubber Corporation. As shown in Fig. 2, the whole test system is composed of the Instron-5865 universal testing machine, the Bullhill2 data acquisition software and a computer.

In the experiment, it is necessary to check that the air spring is airtight after inflated with a small amount of air firstly. Then, the air spring is inflated with different initial air pressures, summarized in Table 1. After that, the test machine is controlled to touch the upper plate of the air spring and set zero. By referring to

[7], the loading and unloading velocity of 10 mm/min and the displacement range of 20 mm are selected in the test.

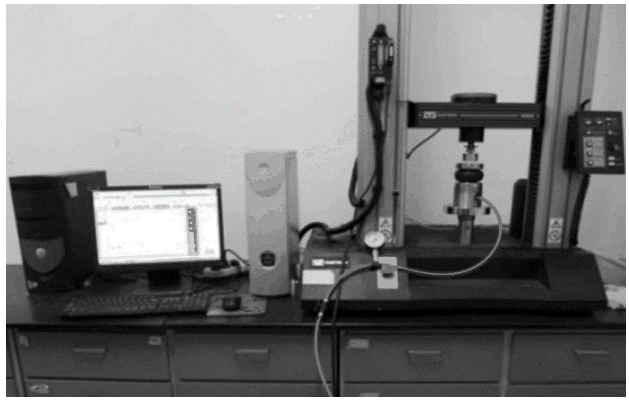

Fig. 2. Experimental setup for testing of the air spring

Table 1. Different initial air pressures of the air spring

Parameter	Value
p_0	0.2 MPa, 0.25 MPa, 0.3 MPa, 0.35 MPa, 0.4 MPa, 0.45 MPa, 0.5 MPa,

The force-displacement curves of the air spring under different given initial air pressures are plotted respectively in Fig. 3. It is worth noting that the force-displacement curves can be approximated to be the cubic curves. According to eg. (7), the stiffness coefficients are obtained in Table 2 after fitting the experimental data with the least square method. As shown in Fig. 4, the fitted and experimental force-displacement curves match exactly.

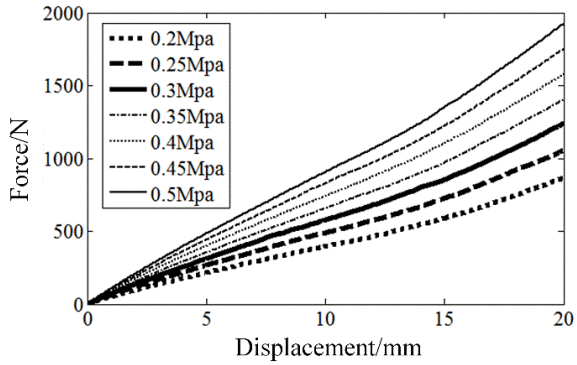

Fig. 3. Force-displacement curves of the air spring under different given initial air pressures

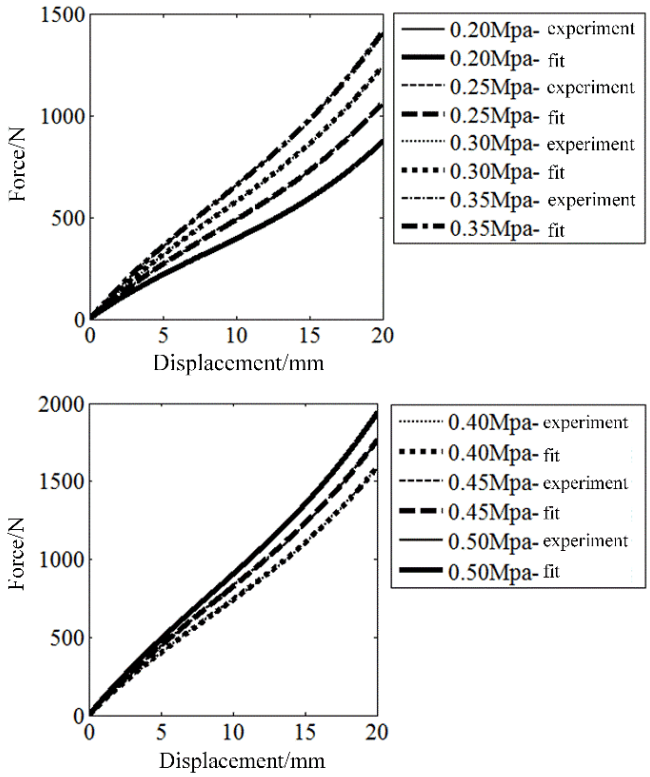

Fig. 4. Fitted (top) and experimental (bottom) force-displacement curves of the air spring

Table 2. Stiffness coefficients of the air spring under different given initial air pressures

Initial air pressure (MPa)	k_3	k_2	k_1	F_0
0.2	0.0813	–2.0179	51.355	1.7637
0.25	0.0959	–2.4404	63.578	0.4903
0.3	0.1046	–2.6944	74.345	–1.9068
0.35	0.1150	–2.9289	83.258	–0.1168
0.4	0.1198	–3.0494	92.496	0.6024
0.45	0.1324	–3.3959	103.24	–2.1531
0.5	0.1394	–3.5161	111.53	–0.5229

3. The proposed nonlinear vibration isolator

3.1. Analytical model of the isolator

The schematic view of the proposed nonlinear vibration isolator is shown in Fig. 5. The three air springs in Fig. 5 are the same type presented in Section 2.

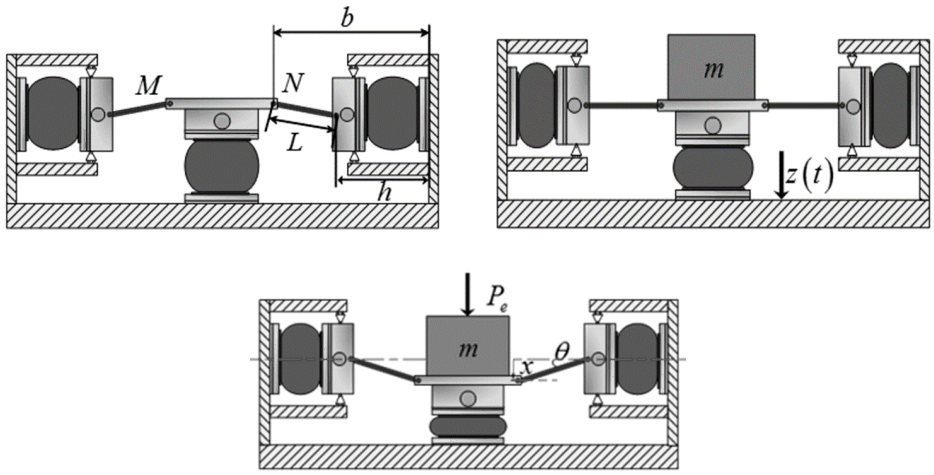

Fig. 5. Schematic representation of the proposed nonlinear vibration isolator: top left–isolator at the initial position, top right–isolator at the equilibrium position, bottom–isolator under axial force

As shown in Fig. 5, top left part, under unloaded condition it can be assumed that the three air springs inflated with the initial air pressure are in relaxing state at the initial position. In this study, it is prospected that the hinge joints M and N of the isolator loaded with an appropriate isolated mass can reach the position $\delta = \delta_0$, which is referred to be an equilibrium position while the bar is forced to be in the horizontal position. Meanwhile, the vertical air spring gets the minimum stiffness and supports the mass by itself at the equilibrium position as shown in Fig. 5, top right part. Based on eq. (8), the deflection δ_0 can be obtained as

$$\delta_0 = -\frac{k_2}{3k_3}\,. \tag{9}$$

In the vertical direction, the mass moves downwards x amounts from the equilibrium position under the applied axial force P_e shown in Fig. 5, bottom part. The restoring force of the isolator F_r includes the restoring force of the vertical air spring F_v and the restoring force generated by the negative stiffness structure F_n, which can be expressed by

$$F_\mathrm{r} = F_\mathrm{v} + F_\mathrm{n} = F_\mathrm{v} - 2F_\mathrm{h}\tan\theta\,. \tag{10}$$

Based on eq. (8), the restoring forces of the vertical air spring F_v and the horizontal air spring F_h can be obtained as follows:

$$F_\mathrm{v} = k_{\mathrm{v}3}\left(x+\delta_0\right)^3 + k_{\mathrm{v}2}\left(x+\delta_0\right)^2 + k_{\mathrm{v}1}\left(x+\delta_0\right) + F_{\mathrm{v}0}\,, \tag{11}$$

$$F_\mathrm{h} = k_{\mathrm{h}3}Q^3 + k_{\mathrm{h}2}Q^2 + k_{\mathrm{h}1}Q + F_{\mathrm{h}0}\,, \tag{12}$$

where $Q = \sqrt{L^2 - x^2} + h - b$.

Then, the restoring force of the isolator can be derived as

$$F_{\mathrm{r}} = k_{\mathrm{v}3}x^3 + k^*_{\mathrm{v}1}x + F^*_{\mathrm{v}0}$$

$$-\frac{2x}{\sqrt{L^2-x^2}}\left(k_{\mathrm{h}3}Q^3 + k_{\mathrm{h}2}Q^2 + k_{\mathrm{h}1}Q + F_{\mathrm{h}0}\right), \tag{13}$$

where

$$k^*_{\mathrm{v}1} = \frac{3k_{\mathrm{v}1}k_{\mathrm{v}3} - k^2_{\mathrm{v}2}}{3k_{\mathrm{v}3}}, \quad F^*_{\mathrm{v}0} = \frac{2k^3_{\mathrm{v}2} - 9k_{\mathrm{v}1}k_{\mathrm{v}2}k_{\mathrm{v}3}}{27k^2_{\mathrm{v}3}} + F_{\mathrm{v}0}\,.$$

It is convenient to define the following non-dimensional parameters:

$$\hat{F}_{\mathrm{r}} = \frac{F_{\mathrm{r}}}{k^*_{\mathrm{v}1}h},\ \hat{x} = \frac{x}{h},\ \lambda_{\mathrm{v}3} = \frac{k_{\mathrm{v}3}h^2}{k^*_{\mathrm{v}1}},\ \hat{F}_{\mathrm{v}0} = \frac{F^*_{\mathrm{v}0}}{k^*_{\mathrm{v}1}h},\ \lambda_{\mathrm{h}1} = \frac{k_{\mathrm{h}1}}{k^*_{\mathrm{v}1}},$$

$$\lambda_{\mathrm{h}2} = \frac{k_{\mathrm{h}2}h}{k^*_{\mathrm{v}1}},\ \lambda_{\mathrm{h}3} = \frac{k_{\mathrm{h}3}h^2}{k^*_{\mathrm{v}1}},\ \hat{F}_{\mathrm{h}0} = \frac{F_{\mathrm{h}0}}{k^*_{\mathrm{v}1}h},\ \alpha = \frac{L}{h},\ \beta = \frac{b}{h}\,. \tag{14}$$

The non-dimensional restoring force can be expressed by

$$\hat{F}_{\mathrm{r}} = \lambda_{\mathrm{v}3}\hat{x}^3 + \hat{x} + \hat{F}_{\mathrm{v}0} -$$

$$-\frac{2\hat{x}}{\sqrt{(\alpha^2-\hat{x}^2)^3}}(\lambda_{\mathrm{h}3}U^3 + \lambda_{\mathrm{h}2}U^2 + \lambda_{\mathrm{h}1}U + \hat{F}_{\mathrm{h}0})\,, \tag{15}$$

where $U = \sqrt{\alpha^2-\hat{x}^2} + 1 - \beta$.

By differentiating eq. (15) with respect to the non-dimensional displacement $\hat{x}$, the non-dimensional stiffness of the isolator can be derived as

$$\hat{k} = 3\lambda_{\mathrm{v}3}\hat{x}^2 + 1 -$$

$$-\frac{2\alpha^2}{\sqrt{(a^2-\hat{x}^2)^3}}\left[\lambda_{\mathrm{h}3}U^3 + \lambda_{\mathrm{h}2}U^2 + \lambda_{\mathrm{h}1}U + \hat{F}_{\mathrm{h}0}\right] + \frac{2\hat{x}^2}{\alpha^2-\hat{x}^2}\left[3\lambda_{\mathrm{h}3}U^2 + 2\lambda_{\mathrm{h}2}U + \lambda_{\mathrm{h}1}\right]. \tag{16}$$

It is prospected that the isolator can get zero stiffness at the equilibrium position i.e. $\hat{x} = 0$ in real operation. Based on eq. (16), the parameters need to satisfy the condition that

$$\frac{2}{\alpha}\left[\lambda_{\mathrm{h}3}\left(\alpha+1-\beta\right)^3\right) + \lambda_{\mathrm{h}2}\left(\alpha+1-\beta\right)^2\Big) + \lambda_{\mathrm{h}1}\left(\alpha+1-\beta\right) + \hat{F}_{\mathrm{h}0}\Big] = 1\,. \tag{17}$$

3.2. Effects of the parameters on the isolator

Based on the above analysis, the internal pressure of the vertical air spring should be fixed for the isolator loaded with a constant mass. It is also found that the non-

dimensional restoring force and stiffness of the isolator are affected by the configurative parameters α and β as well as the internal pressure of the horizontal air spring. Besides, a conclusion can be drawn from eq. (17) that the value of the configurative parameter β increases as α increases to enable the isolator to get the zero stiffness at the equilibrium position, while the internal pressure of the horizontal air spring is fixed. By using the values listed in Table 3, effects of the configurative parameters α and β on the isolator are shown in Fig. 6. It is worth noting that the values of α and β in Table 3 are derived by eqs. (17). By observing Fig. 6, one can conclude that the isolator possesses smaller stiffness in the neighborhood of the equilibrium position and larger region of smaller stiffness around the equilibrium position with increasing α and β when the internal pressures of the air springs are fixed.

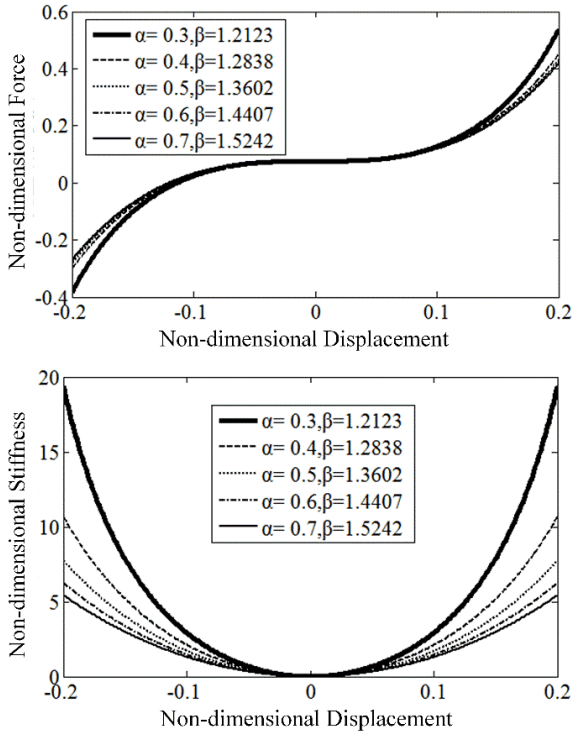

Fig. 6. Effects of the configurative parameters α and β on the isolator: top–non-dimensional force-displacement curves, bottom–non-dimensional stiffness-displacement curves

Figure 7 shows the non-dimensional force-displacement and stiffness-displacement curves with different internal pressures of the horizontal air spring, in which the configurative parameters α and β are fixed. The values of the parameters are listed in Table 4. As the internal pressure increases, the stiffness of the isolator decreases at the same position, which means that larger internal pressure of the horizontal air spring results in larger negative stiffness in the vertical direction. Note that the region of negative stiffness occurs when the internal pressure larger than 0.4 MPa.

Table 3. Values of the fixed internal pressures and the changing configurative parameters

Parameters	Value
Internal pressure of vertical air spring	0.25 MPa
Internal pressure of horizontal air spring	0.4 MPa
Configurative parameters	$\alpha = 0.3$, $\beta = 1.2123$; $\alpha = 0.4$, $\beta = 1.2838$; $\alpha = 0.5$, $\beta = 1.3602$; $\alpha = 0.6$, $\beta = 1.4407$; $\alpha = 0.7$, $\beta = 1.5242$;

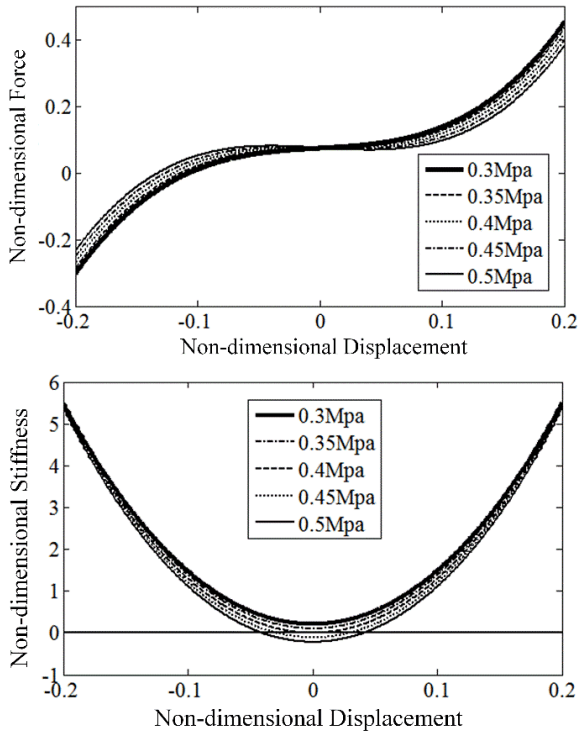

Fig. 7. Effects of the internal pressure of horizontal air spring on the isolator: top–non-dimensional force-displacement curves, bottom–non-dimensional stiffness-displacement curves

Table 4. Values of the changing internal pressures and the fixed configurative parameters

Parameters	Value
Internal pressure of vertical air spring	0.25 MPa
Internal pressure of horizontal air spring	0.3 MPa, 0.35 MPa, 0.4 MPa, 0.45 MPa, 0.5 MPa
Configurative parameters	$\alpha = 0.7$, $\beta = 1.5242$

4. Dynamic analysis

4.1. Approximation of the restoring force

The expression of the non-dimensional restoring force by substituting eq. (17) into (15) is very complicated and can be expanded by using the Taylor series at the equilibrium position. Then, the non-dimensional restoring force of the isolator can be rewritten as

$$\hat{F}_{\mathrm{rapp}} = \hat{F}_{\mathrm{v0}} + \gamma \hat{x}^3 \,, \tag{18}$$

where $\hat{F}_{\mathrm{rapp}}$ is the non-dimensional restoring force after approximation and the coefficient γ is

$$\gamma = \lambda_{\mathrm{v3}} + \frac{1}{\alpha^2}\left[3\lambda_{\mathrm{h3}}\left(\alpha + 1 - \beta\right)^2 + 2\lambda_{\mathrm{h2}}\left(\alpha + 1 - \beta\right) + \lambda_{\mathrm{h1}} - \frac{1}{2}\right] . \tag{19}$$

4.2. Dynamic modeling and solution

Going back to Fig. 5, bottom left part. It is assumed that the isolator loaded with an appropriate mass can keep balance at the equilibrium position $\hat{x} = 0$. And the stiffness of the isolator is zero at this position. The quantity of the mass should satisfy the condition

$$mg = F^*_{\mathrm{v0}} \,. \tag{20}$$

Then the nonlinear system which is configured by the nonlinear isolator and the isolated mass is exposed to a harmonic displacement excitation $z\left(t\right) = Z\cos\left(\omega t\right)$. By using the Newton's second law of motion, the dynamic equation of the nonlinear system can be expressed by

$$m\ddot{u} + c\dot{u} + k^*_{\mathrm{v1}} h\gamma \hat{u}^3 = m\omega^2 Z\cos\left(\omega t\right) \,, \tag{21}$$

where $u = x - z$ is the relative displacement. Combining it with eq. (14) and introducing the following non-dimensional parameters

$$\tau = \omega_{\mathrm{n}} t,\ \Omega = \frac{\omega}{\omega_{\mathrm{n}}},\ \omega_{\mathrm{n}} = \sqrt{\frac{k^*_{\mathrm{v1}}}{m}},\ \hat{u} = \frac{u}{h},\ \xi = \frac{c}{2m\omega_{\mathrm{n}}},\ \hat{Z} = \frac{Z}{h}, \tag{22}$$

eq. (19) can be rewritten as the non-dimensional form:

$$\hat{u}'' + 2\xi\hat{u}' + \gamma\hat{u}^3 = \Omega^2\hat{Z}\cos(\Omega\tau)\ . \tag{23}$$

Considering that the nonlinear system may possess strong nonlinearity and the frequency of response is predominantly the same as that of the harmonic excitation, the Harmonic Balance Method is employed to get the approximate steady-state solution. The steady-state solution of the nonlinear system can be assumed to be

$$\hat{u} = A\cos(\Omega\tau + \varphi)\ . \tag{24}$$

After substituting eq. (24) into eq. (22) and neglecting the third harmonic and equating the coefficients of the same harmonics, the steady-state solution is found to satisfy

$$-\Omega^2 A + \frac{3}{4}\gamma A^3 = \Omega^2\hat{Z}\cos(\varphi)\,,\quad -2\xi\Omega A = \Omega^2\hat{Z}\sin(\varphi)\ . \tag{25}$$

Combining eqs. (25), one can get the implicit amplitude frequency equation of the nonlinear system

$$\frac{9}{16}\gamma^2 A^6 - \frac{3}{2}\gamma\Omega^2 A^4 + \Omega^2\left(\Omega^2 + 4\xi^2\right)A^2 - \Omega^4\hat{Z}^2 = 0\,. \tag{26}$$

Then, the absolute displacement transmissibility is defined as the ratio of the magnitude of the absolute displacement of the mass to that of the displacement excitation. It can be given as

$$T_{\mathrm{ns}} = \frac{|\hat{x}|}{|\hat{z}|} = \frac{|\hat{u}+\hat{z}|}{|\hat{z}|} = \frac{\sqrt{A^2 + \hat{Z}^2 + 2A\hat{Z}\cos(\varphi)}}{\hat{Z}}\,, \tag{27}$$

where $\cos(\varphi)$ is defined by the first equation in (25).

As discussed above, the restoring force in the vertical direction given by the negative stiffness structure is zero at the equilibrium position. If the negative stiffness structure is removed at this position, the vertical air spring can support the mass with the exact same deflection. Here, the system configured by the vertical air spring and the mass is called the single air spring system. By introducing the same non-dimensional parameters, the dynamic equation of the single air spring system under the same excitation can be derived as

$$\hat{u}'' + 2\xi\hat{u}' + \lambda_{\mathrm{v}3}\hat{u}^3 + \hat{u} = \Omega^2\hat{Z}\cos(\Omega\tau)\ . \tag{28}$$

For the single air spring system, the steady-state solution can be obtained by following the procedure above. The steady-state solution needs to satisfy

$$-\Omega^2 A + \frac{3}{4}\lambda_{\mathrm{v}3}A^3 + A = \Omega^2\hat{Z}\cos(\varphi)\,,\quad -2\xi\Omega A = \Omega^2\hat{Z}\sin(\varphi)\ . \tag{29}$$

The absolute displacement transmissibility of the single air spring system can be expressed by

$$T_{\text{sass}} = \frac{|\hat{x}|}{|\hat{z}|} = \frac{|\hat{u} + \hat{z}|}{|\hat{z}|} = \frac{\sqrt{A^2 + \hat{Z}^2 + 2A\hat{Z}\cos(\varphi)}}{\hat{Z}}, \tag{30}$$

where $\cos(\varphi)$ is defined by the first equation in (29).

4.3. Effects of the system imperfections on the absolute displacement transmissibility

Note that the internal pressure of the vertical air spring is set to be 0.25 MPa, the internal pressure of the horizontal air spring is set to be 0.4 MPa, and the configurative parameters $\alpha = 0.7$ and $\beta = 1.5242$ are selected. The absolute displacement transmissibility results of the two systems under the same system imperfections are plotted in Fig. 8 for comparison convenience.

Figure 8 shows the absolute displacement transmissibility of the two systems with different excitation amplitudes $\hat{Z}$ and a fixed damping ratio $\xi = 0.04$. It can be seen that the absolute displacement transmissibility of the two systems are affected obviously with the increasing excitation amplitude. Larger excitation amplitude leads to larger peak amplitude of the absolute displacement transmissibility. And unbounded absolute displacement transmissibility may occur when the excitation amplitude is relatively large. Moreover, the isolation performance of the nonlinear system can be superior or inferior to the single air spring system depending on the frequency range and excitation amplitude. For the two systems with same excitation amplitude, the absolute displacement transmissibility of the nonlinear system is larger than that of the single air spring system at lower frequencies. When the excitation frequency is larger than the jump-down frequency of the nonlinear system, the absolute displacement transmissibility of the nonlinear system will get smaller than that of the single air spring system in a large frequency range. And the superiority of the nonlinear system to the single air spring system is getting lower at higher frequencies. Besides, the least frequency of the nonlinear system where a vibration can be isolated increases as the excitation amplitude increases, which means that the excitation amplitude should be limited in order to get a better isolation performance of the nonlinear system.

Figure 9 shows the absolute displacement transmissibility of the two systems with different damping ratios ξ and a fixed excitation amplitude $\hat{Z} = 0.014$. By observing Fig. 4, the interactive feature of the absolute displacement transmissibility between the two systems at different frequency regions with increasing damping ratio is similar with that with decreasing excitation amplitude. It is also found that larger damping ratio leads to smaller peak amplitude of the absolute displacement transmissibility of the two systems. If the damping ratio is large enough, peak amplitudes of the absolute displacement transmissibility for the nonlinear system will not occur. Meanwhile, the unstable regions of the two systems are getting smaller as the damping ratio increases. Based on above analysis, an appropriate

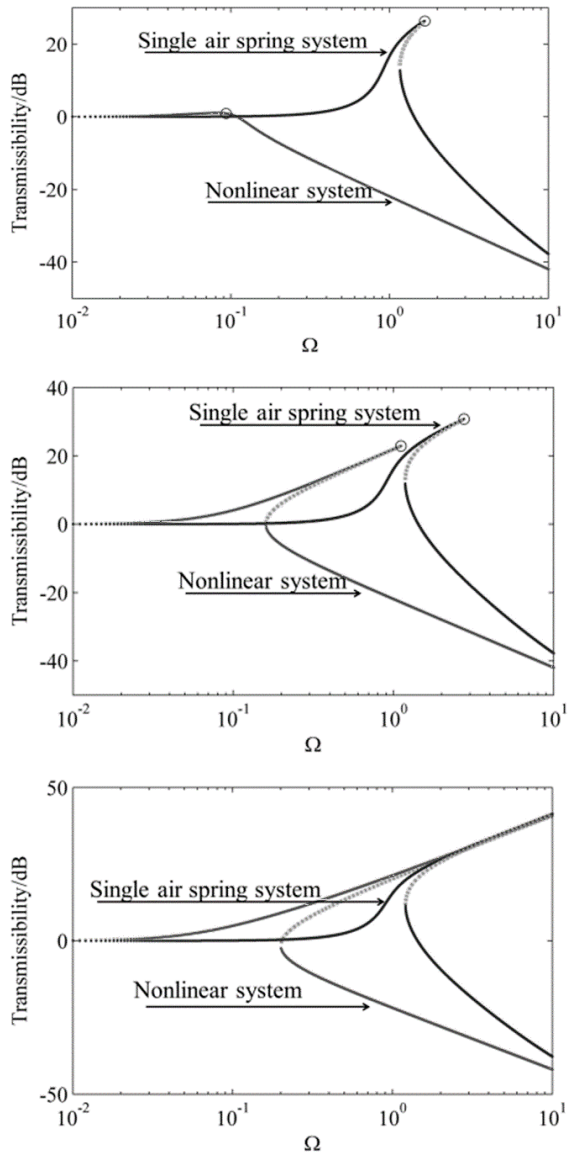

Fig. 8. Absolute displacement transmissibility of the two systems with different excitation amplitudes; 'dotted line' denotes unstable solution and 'o' denotes peak amplitude of the transmissibility: top–$\hat{Z} = 0.012$, middle–$\hat{Z} = 0.014$, bottom–$\hat{Z} = 0.016$

damping ratio should be chosen to improve the vibration isolation performance of the nonlinear system.

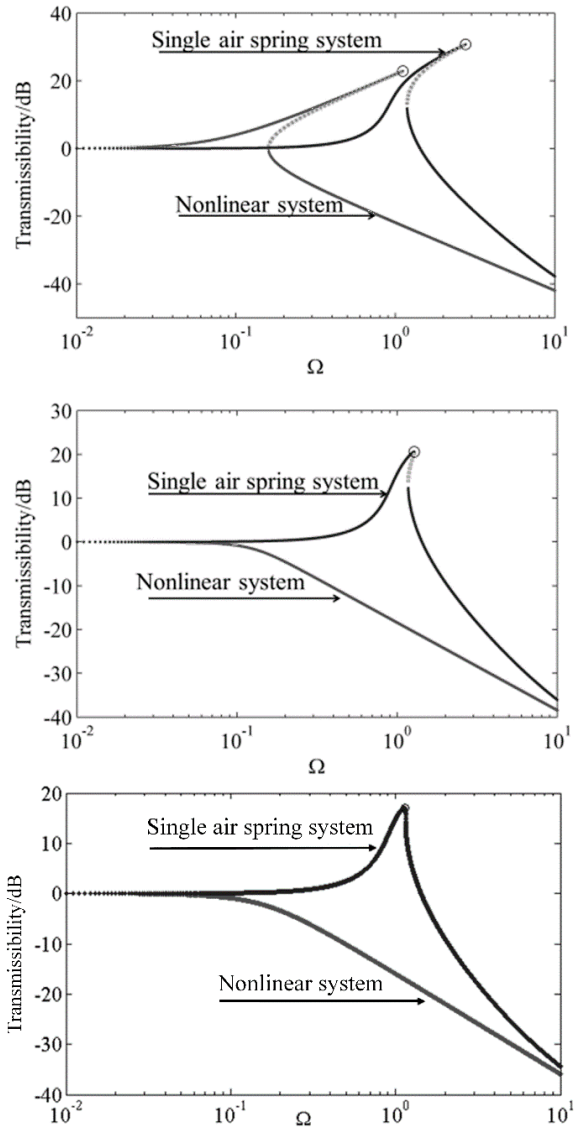

Fig. 9. Absolute displacement transmissibility of the two systems with different damping ratios; 'dotted line' denotes unstable solution and 'o' denotes peak amplitude of the transmissibility: top–$\xi = 0.04$, middle–$\xi = 0.06$, bottom–$\xi = 0.08$

5. Summary

In this paper, we introduce the theoretical investigation of a passive nonlinear vibration isolator. The conclusion can be drawn that the nonlinear system can ex-

hibit excellent isolation performance at lower frequency compared with the single air spring system without the negative stiffness structure. Meanwhile, smaller peak amplitude of the absolute displacement transmissibility and frequency where a vibration can be isolated would be obtained for the nonlinear system with appropriate excitation amplitude and larger damping ratio.

References

[1] R. A. Ibrahim: *Recent advances in nonlinear passive vibration isolators.* Journal of Sound and Vibration *314* (2008), Nos. 3–5, 371–452.

[2] P. Alabuzhev, A. Gritchin, L. Kim, G. Migirenko, V. Chon, P. Stepanov: *Vibration protecting and measuring systems with quasi-zero stiffness.* Hemisphere Publishing Corporatin, Taylor and Francis Group, New York (1989).

[3] A. Carrella: *Passive vibration isolators with high-static-low-dynamic-stiffness.* Ph.D. Thesis, University of Southampton, Institute of Sound and Vibration Research, UK (2008).

[4] T. D. Le, K. K. Ahn: *A vibration isolation system in low frequency excitation region using negative stiffness structure for vehicle seat.* Journal of Sound and Vibration *330* (2011), No. 26, 6311–6335.

[5] X. T. Liu, X. C. Huang, H. X. Hua: *On the characteristics of a quasi-zero stiffness isolator using euler buckled beam as negative stiffness corrector.* Journal of Sound and Vibration *332* (2013), No. 14, 3359–3376.

[6] L. S. Meng, J. G. Sun, W. J. Wu: *Theoretical design and characteristics analysis of a quasi-zero stiffness isolator using a disk spring as negative stiffness element.* Shock and Vibration (2015), paper 1–19.

[7] M. N. Fox, R. L. Roebuck, D. Cebon: *Modelling rolling-lobe air springs.* International Journal of Heavy Vehicle Systems *14* (2007), No. 3, 254–270.

[8] P. K. Wong, Z. C. Xie, T. Xu, J. Zhao, F. He: *Analysis of automotive rolling lobe air spring under alternative factors with finite element model.* Journal of Mechanical Science and Technology *28* (2014), No. 12, 5069–5081.

Received April 30, 2017